Global and Planetary Change 109 (2013) 46–63

Contents lists available at ScienceDirect

Global and Planetary Change

journal homepage: www.elsevier.com/locate/gloplacha

Precipitation projections for Spain by means of a weather typing statistical method

J. Osca *, R. Romero, S. Alonso

Meteorology Group, Departament de Física, Universitat de les Illes Balears, Palma de Mallorca, Spain

ARTICLE INFO

Article history:
Received 31 October 2012
Revised 26 June 2013
Accepted 1 August 2013
Available online 9 August 2013

Keywords:
Spain
precipitation downscaling
rainfall patterns
circulation types
weather generation
stochastic method

ABSTRACT

This study develops a weather typing stochastic method for the climatic prediction of rainfall in Peninsular Spain and the Balearic Islands during the 21st century. Cluster analysis is applied to the geopotential height fields with the purpose of classifying the atmospheric states into distinct daily circulation patterns. The same kind of analysis is performed on the rainfall distributions, obtaining the corresponding daily rainfall patterns. It is possible to establish a suitable association between each of the circulation types and the rainfall patterns. This circulation–rainfall link becomes the essence of our downscaling method, which will allow the "reconstruction" of the accumulated rainfall field from a generated sequence of daily rainfall patterns. This is done with the support of a statistical weather generator using the daily patterns of atmospheric circulation provided by different GCMs as input. The weather typing approach and the weather generator strategy interrelate in a novel and unique way different from any previous method. The downscaling method is first subjected to calibration, using reanalysis circulation as input, from which the optimal number of atmospheric and rainfall patterns to perform the projection is found. Later on the method is subjected to validation, using GCMs' daily atmospheric circulation as input, in order to test its robustness. The final part of the study focuses on the analysis and intercomparison of future precipitation projections for the 21st century under the A1B emission scenario from five different GCMs. A substantial drying of about 30% is foreseen at the end of the century in Spain compared to present, although with a nonuniform pattern in space and time as the century progresses.

1. Introduction

Global warming is the measured average temperature increase of the Earth's lower troposphere in the 20th century attributed to human activities (Solomon et al., 2007). The increasing interest in global warming has been motivated by its impact on the Earth's ecosystem and its available resources and, more importantly, on the human societies. Although the global warming effect has been widely studied (e.g. Harin et al., 2007; Durack and Wijffels, 2010; DelSole et al., 2011) it can lead to a more generalized climatic change with a profound impact on the atmosphere dynamics and precipitation patterns (Held, 1993; Romps, 2011; Chou et al., 2012). The Iberian Peninsula and Balearic Islands, depicted in Fig. 1a, is a region of particular interest in studies of climate change. This zone is subjected to extreme seasonal contrasts and as a result of anthropogenic emissions of greenhouse gases (GHG) and its geographical location, large changes on temperature and precipitation are expected throughout the century (Solomon et al., 2007). Global Climate Models (GCMs) have been used to study the changes in precipitation globally and at a continental scale (Dai, 2006; Solomon et al., 2007). However, the complex topography of the Mediterranean region and the relatively low resolution and reliability of the projections provided by GCMs have raised in the case of precipitation the need of developing a new set of downscaling methods that can provide useful predictions with higher resolution (Giorgi and Mearns, 1991). That set of methods is mainly distributed in two classes: dynamical and statistical methods. Dynamical methods rely on the knowledge of the atmospheric physics to perform simulations of the atmospheric circulation nested in the GCMs. On the other hand, statistical methods rely on statistical correlations that can be deduced between reanalysis data and the databases of the observed variables at higher resolution. This second kind of methods are less demanding in terms of computer resources and provide alternative future projections that can be compared with the projections generated by the more expensive dynamical methods.

The method developed in this study can be integrated into the second class, i.e. statistical methods. Our main goal is to generate daily precipitation time series that are consistent with the climate model tendencies they are derived from. The series are generated at daily scale with the triple objective of: (i) producing data that has the potential to be aggregated and analyzed in different ways as a base for future work, (ii) easing the comparison with the results provided by dynamical methods and (iii) providing adequate input to further impact models that depend on the amount of precipitation down to the daily scale. As explained in the next section, this goal leads to the use of a stochastic weather generator. Willems and Vrac (2011) suggest a classification of statistical methods into transfer function approaches, stochastic weather

* Corresponding author. Tel.: +34 971173233; fax: 34 971173426.
E-mail address: javier.osca@uib.es (J. Osca).

0921-8181/$ – see front matter © 2013 Elsevier B.V. All rights reserved.
http://dx.doi.org/10.1016/j.gloplacha.2013.08.001

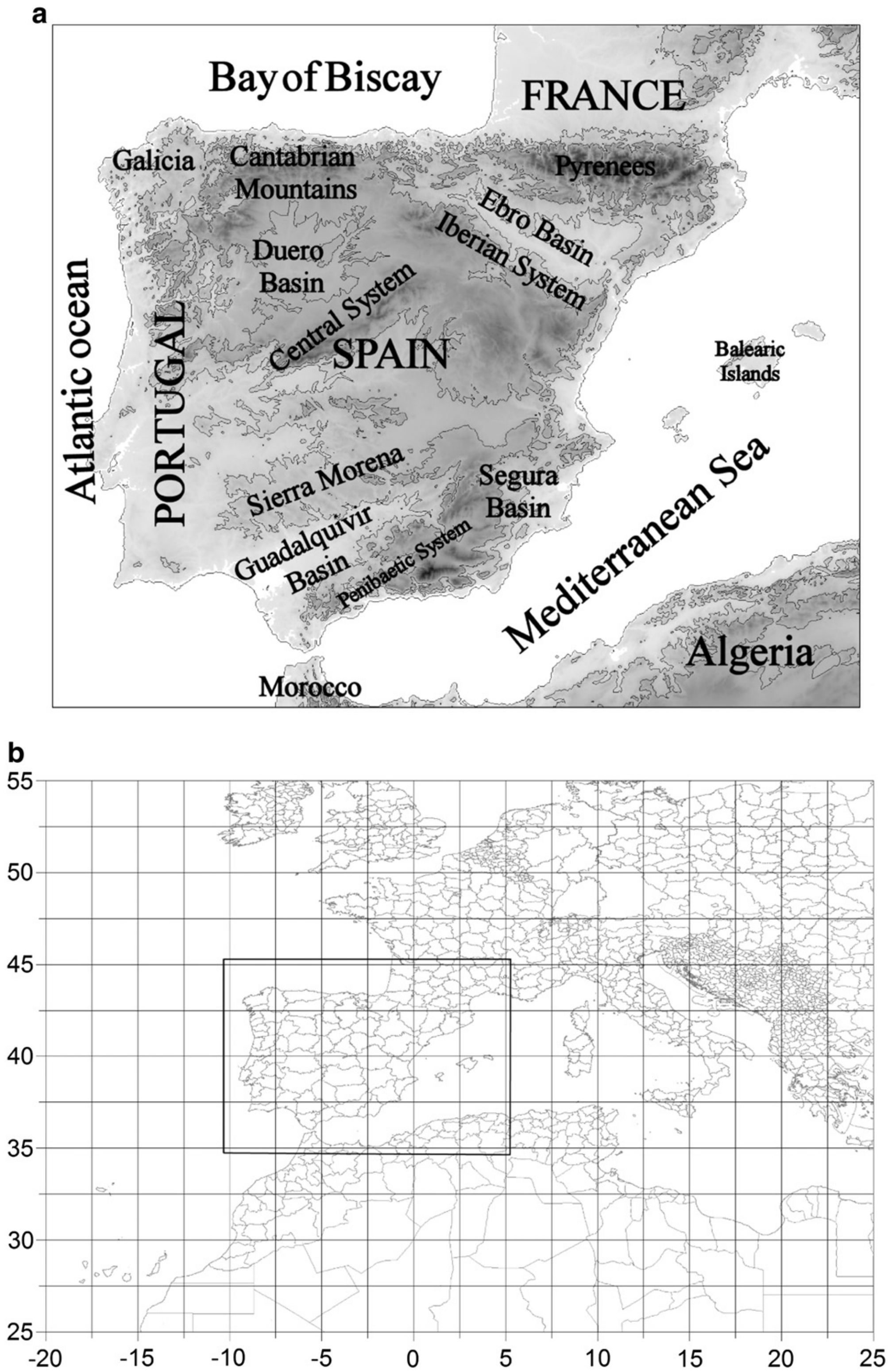

Fig. 1. a) Main orographic features of Peninsular Spain and Balearic Islands. The domain shown corresponds to the geographical area used for the atmospheric circulation classification. b) 2.5° resolution GCM data grid.

generators and weather typing approaches. The present method uses weather typing and a weather generator and therefore it can be formally classified as a hybrid type of these two classes. However, both approaches interrelate in a novel way that has its own strengths and weaknesses as it will be discussed.

Ribalaygua and Borén (1995) and Romero et al. (1999a) used clustering methods to analyze the distribution of precipitation over Spain and the Mediterranean, respectively. There are also studies using statistical information linking synoptic atmospheric circulation patterns and different surface weather parameters (e.g. Gutiérrez et al., 2004;

Table 1
GCMs used for the precipitation projections.

GCM	Abbreviation
Bjerknes Institute for Climate Research BCM 2.0	BCM2
Centre National de Recherches Météorologiques CNRM-CM3	CNCM3
Centre National de Recherches Météorologiques CNRM-CM33	CNCM33
Max Planck Institute (Hamburg) ECHAM5	MPEH5
Max Planck Institute (Hamburg) ECHAM5C	MPEH5C
Institute for Meteorology ECHO-G Middle atmosphere model	EGMAM
Institute for Meteorology ECHO-G Middle atmosphere model v2	EGMAM2
Hadley Center HADGEM	HADGEM
Hadley Center HADGEM2	HADGEM2
Hadley Center HADCM3C	HADCM3C
Institute Pierre Laplace IPCM4	IPCM4

Benestad et al., 2008) and precipitation in particular (e.g. Sumner et al., 2003). Gutiérrez et al. (2004) offer information about multiple statistical methods including methods in which the applied similarity criterion is the distance between the spatial patterns of the physical variable under consideration, as in Zorita and von Storch (1999). On the other hand, Duda et al. (2001) present many methods to perform this classification. Gutiérrez et al. (2004) also provide information on stochastic methods such as Markov's chains and stochastic weather generators, widely used in different precipitation prediction studies like those of Jeong et al. (2011), Chen et al. (2010), Fu et al. (in press) or Sørup et al. (2012).

The present method is heavily influenced and, in fact, can be considered an evolution of the method described in Sumner et al. (2003). That work carried out a classification of different circulation types or atmospheric patterns (APs) and the resulting daily precipitation distributions or rainfall patterns (RPs) that affect the Spanish Mediterranean area. By consideration of a training data base the study was able to compute the frequency of each RP within a given AP, i.e. to find the conditional probability matrix. Later on, this information was used to make projections of the future precipitation on the basis of the APs' occurrence in a GCM transient simulation. A novel feature was the capability of the method to correct the inherent biases of the used GCM by means of the comparison of AP frequencies with those found in reanalysis data for a same control period. However, Sumner et al. (2003) method does not account for the possible effects associated with changes in predictor variable's magnitude and only produces mean precipitation maps for a future time slice instead of the more desirable daily distributions. These limitations are overcome in the present approach, with the additional advantage of its wider application to several GCMs and consideration of updated emission scenarios (SRES, Nakicenovic et al., 2000). The method will be applied to explore

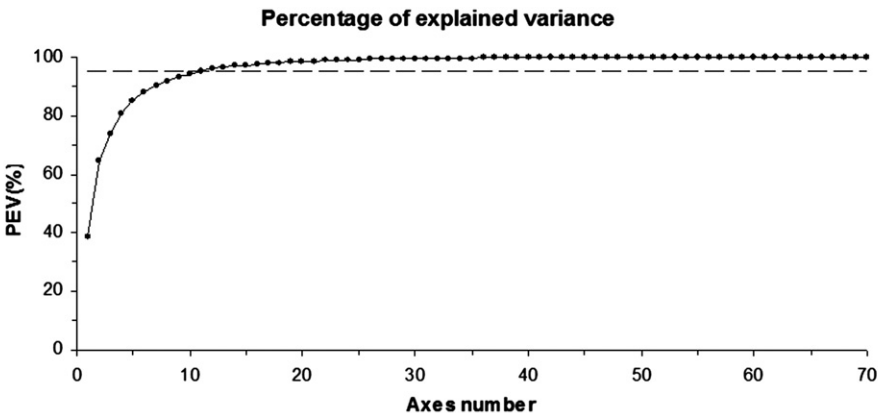

Fig. 2. Percentage of explained variance as function of the number of axes or principal components considered in the PCA of 500 hPa and 850 hPa geopotentials. Both variables are previously standardized in order to be analyzed simultaneously. The overall explained variance raises quickly and more than 95% can be explained with only eleven principal components.

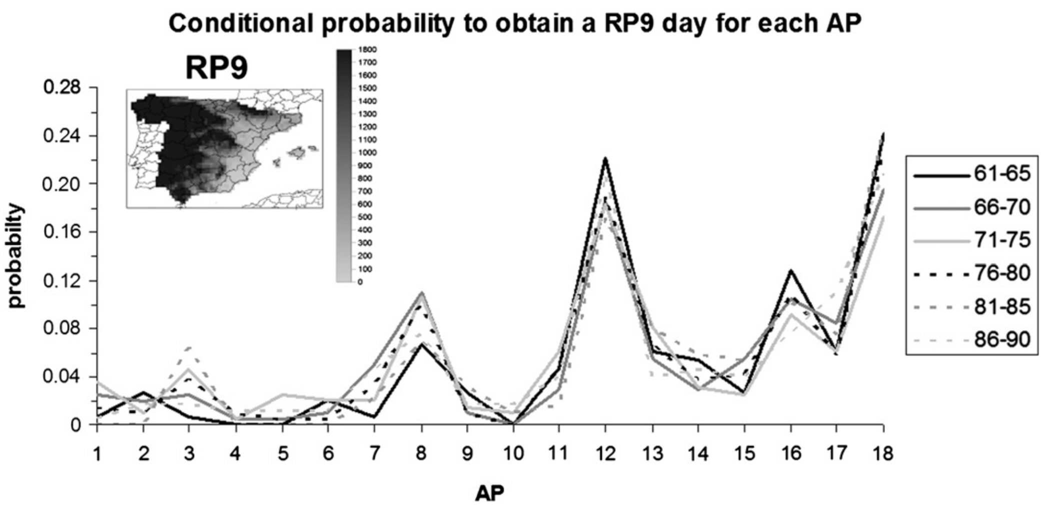

Fig. 3. Probability of occurrence of RP 9 for each atmospheric pattern. Rain pattern from Fig. 4 is depicted as annual accumulated precipitation in mm. Note the stationarity hypothesis as no temporal tendency arises along the sequence of 5-year data.

the effects of climate change on precipitation over Peninsular Spain and the Balearic Islands during the 21st century.

To this end, the intricacies of the method and the data sets used to feed it are first presented (Section 2). The technique depends on two free parameters that must be determined through a calibration process. Section 3 describes the calibration procedure which serves also to learn the basic characteristics and limitations of the downscaling method. This calibration uses reanalysis data while in Section 4 we carry out the validation of the downscaling method using GCM data for a reference period. Finally, Section 5 presents and discusses the future precipitation projections.

2. Data base and methodology

2.1. Atmospheric and precipitation data

The atmospheric circulation data available to implement the training phase of the method are the ERA40 grid reanalyses developed by the European Centre for Medium-Range Weather Forecasts (ECMWF) (Uppala et al., 2005). This gridded data contains geopotential, temperature, relative humidity and horizontal wind components with a spatial resolution of 2.5° in both latitude and longitude. A thirty year period from 1st January 1961 to 31th December 1990 was

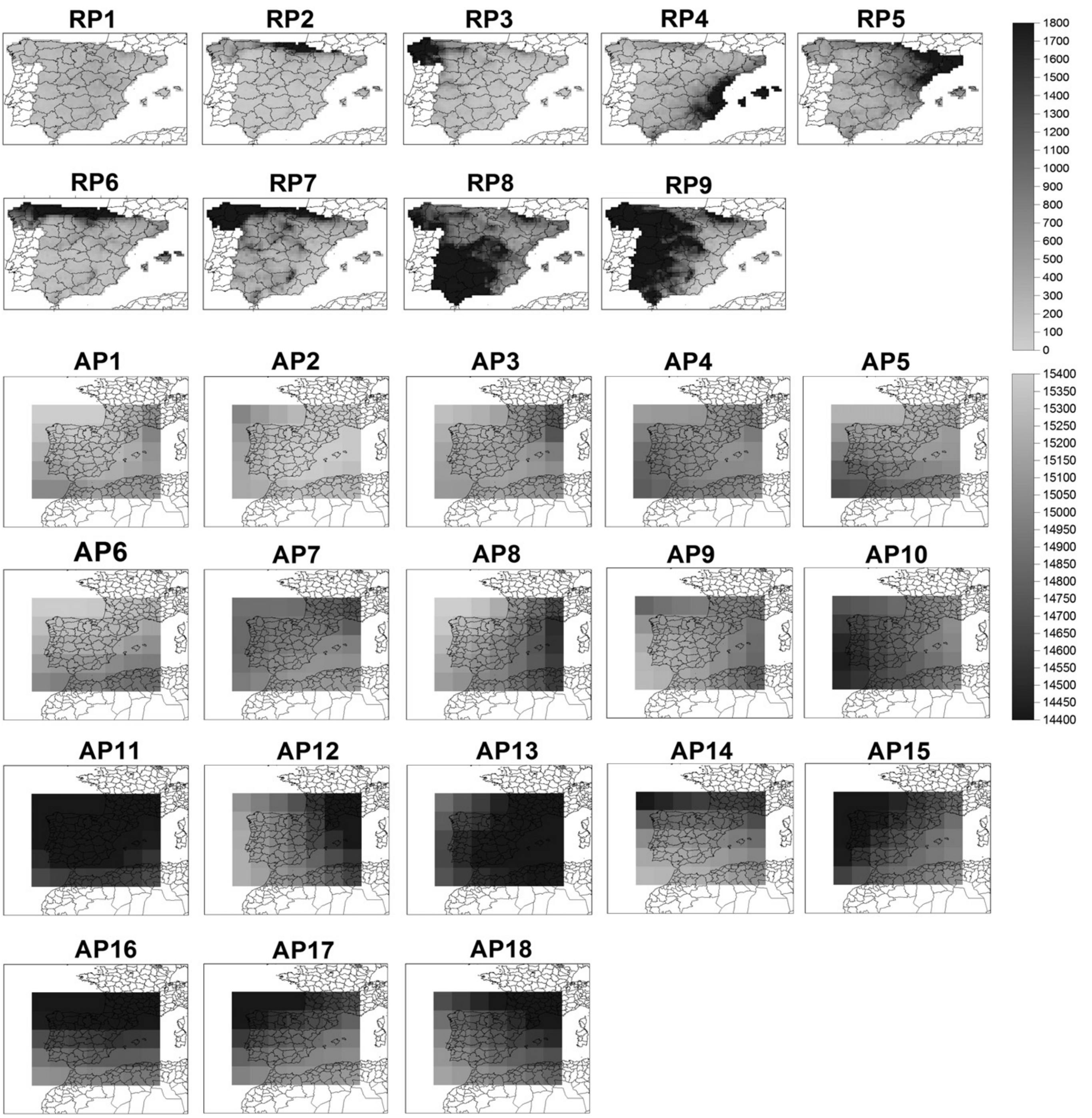

Fig. 4. Example of 9 RPs and 18 APs classification obtained by means of a k-means cluster analysis. RP composites are presented as annual accumulated precipitation in mm. AP composites are presented only for the geopotential at 850 hPa, in m^2/s^2.

Table 2
Example of a conditional probability table, corresponding to the classification shown in Fig. 4. Note that RP0 corresponds to a zero rain class at every point of the grid.

	RP1	RP2	RP3	RP4	RP5	RP6	RP7	RP8	RP9	RP0
AP1	0.6035	0.0623	0.0050	0.1322	0.0424	0.0424	0.0050	0.0474	0.0050	0.0549
AP2	0.6000	0.0185	0.0831	0.0338	0.0431	0.0462	0.0431	0.0615	0.0369	0.0338
AP3	0.5821	0.1227	0.0050	0.0746	0.0846	0.0630	0.0050	0.0348	0.0083	0.0199
AP4	0.5471	0.0118	0.0059	0.0853	0.1176	0.0176	0.0176	0.1353	0.0529	0.0088
AP5	0.4671	0.0035	0.0069	0.2215	0.0519	0.0311	0.0035	0.1834	0.0138	0.0173
AP6	0.4613	0.0179	0.0149	0.3482	0.0655	0.0357	0.0000	0.0149	0.0060	0.0357
AP7	0.4586	0.0303	0.0222	0.0343	0.1919	0.0687	0.0263	0.1131	0.0444	0.0101
AP8	0.3912	0.1640	0.0189	0.2019	0.0158	0.1577	0.0079	0.0174	0.0000	0.0252
AP9	0.3732	0.0739	0.1725	0.0704	0.0352	0.0704	0.1092	0.0387	0.0493	0.0070
AP10	0.3653	0.0133	0.0213	0.1387	0.1360	0.0187	0.0267	0.2080	0.0720	0.0000
AP11	0.1977	0.0610	0.0116	0.1105	0.3459	0.1308	0.0727	0.0436	0.0262	0.0000
AP12	0.2120	0.2999	0.0564	0.0688	0.0248	0.2413	0.0643	0.0192	0.0090	0.0045
AP13	0.1649	0.0632	0.0175	0.2982	0.1298	0.2526	0.0351	0.0386	0.0000	0.0000
AP14	0.2555	0.0501	0.2516	0.0064	0.0565	0.0603	0.1682	0.0347	0.1078	0.0090
AP15	0.2458	0.0428	0.1045	0.0226	0.0938	0.0546	0.0914	0.1651	0.1734	0.0059
AP16	0.1306	0.0733	0.1403	0.0185	0.1571	0.0997	0.2136	0.0609	0.1041	0.0018
AP17	0.1828	0.0442	0.1968	0.0029	0.1024	0.0612	0.1570	0.0766	0.1724	0.0037
AP18	0.1907	0.1915	0.0865	0.0441	0.1178	0.1915	0.1154	0.0313	0.0256	0.0056

chosen, with the fields available at 00 UTC on a daily basis. As the first step of the procedure, the synoptic-scale circulation over the geographical window shown in Fig. 1b was classified in atmospheric patterns. This domain (35 grid points) is large enough to fully encompass Peninsular Spain and the Balearic Islands but sufficiently small to avoid contamination of the regional AP classification from remote areas. Further tests of the method with a domain slightly larger or shifted to the NE and SW has proven few differences, thus the domain selection is robust. The classification was carried out using two variables: 500 hPa and 850 hPa geopotential fields. This selection is motivated by the work of Sumner et al. (2003), who concluded the feasibility with these two fields of capturing the mid and low tropospheric mechanisms responsible for the precipitation generation or suppression.

Additionally, eleven global circulation models were available for the validation phase of the study as well as for the production of the future precipitation projections. The same variables and domain described above were extracted from these GCMs, which belong to six model families and are listed in Table 1.

On the other hand, the precipitation data used to carry out the training of the algorithm come from the so-called Spain02 grid. Spain02 is a regular 0.2° (approx. 20 km) horizontal resolution daily precipitation grid covering Peninsular Spain and the Balearic Islands and spanning

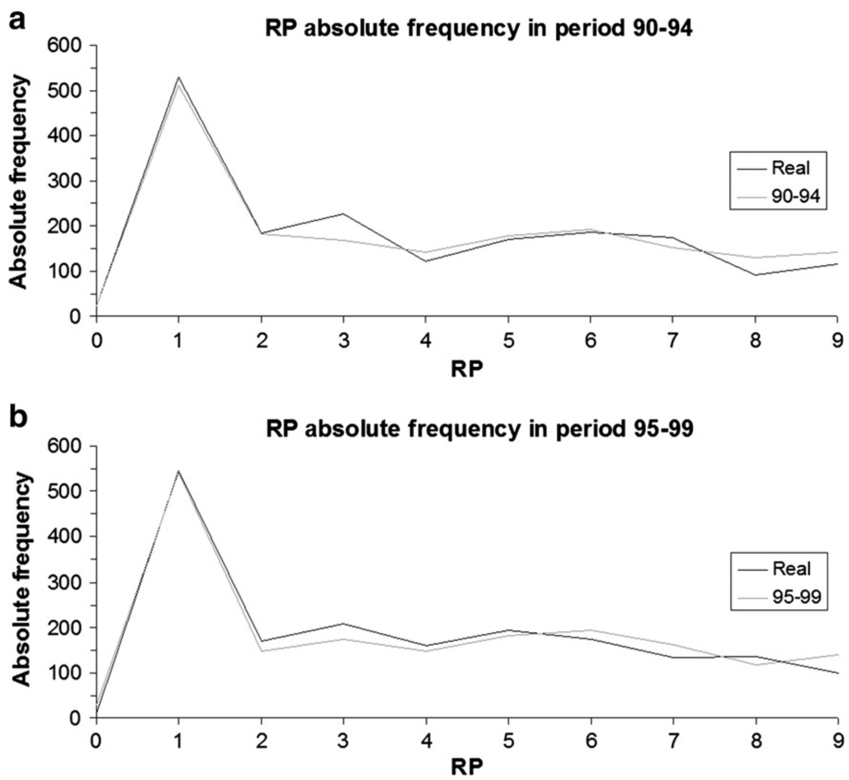

Fig. 5. a) Absolute frequencies of the different rainfall patterns in the period 90–94 for real and predicted precipitation. Note the good agreement between both distributions. Kolmogorov–Smirnov test p-values for the comparison between real and synthetic distributions attain 73.58%. b) The same but for the period 95–99 but with Kolmogorov–Smirnov test p-values for the comparison of 98.58%. In both figures the null hypothesis is that both distributions are equal. The test would reject the null hypothesis if performs under 5% of significance level.

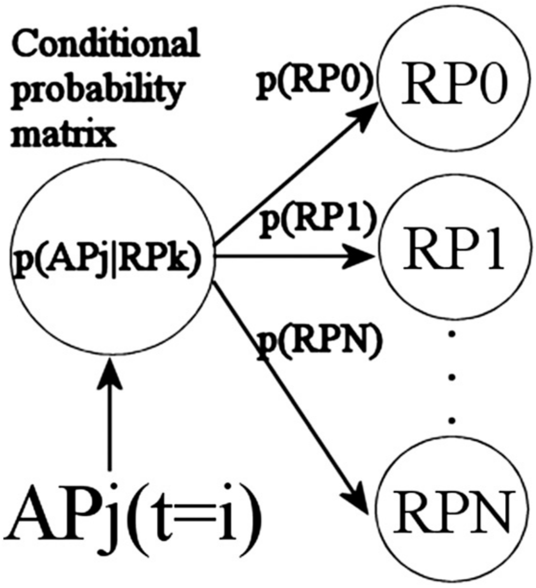

Fig. 6. Weather generator working schematic. In a day t=i an APj is found, thus the probability distribution of RPs conditional to this AP can be found in the probability matrix M. One of the RPs is selected in a random way but in agreement with the observed distribution.

the period from 1950 to 2008. This grid was built by the Universidad de Cantabria Meteorology Group (Herrera et al., 2010) using a Kriging interpolation method from a network of about 2500 irregularly-distributed quality-controlled stations from the Spanish Meteorological Agency (AEMET).

2.2. Classification and probability matrix

To relate the atmospheric circulation with daily precipitation, first the data sets are grouped in *atmospheric patterns* (APs) and *rainfall patterns* (RPs), respectively. Classification is a common way of analyzing structured data (Fovell and Fovell, 1993); the clustering algorithm used is the non-hierarchical k-means method (Anderberg, 1973), as implemented in the *MeteoLab* library (Cofiño et al., 2010). This classification method has been previously used by the authors for precipitation in Romero et al. (1999a) and for atmospheric circulation in Romero et al. (1999b). K-means method relies on the representation of the variable under analysis on an n-dimensional space where each axis is a station (i.e. a grid point) and each day is a point within the space. Days are intercompared by means of the Euclidean distance and the method seeks the grouping of days that tends to minimize intracluster distance and maximize intercluster distance. The particular number of categories in which the data is grouped is an important parameter of the classification process, therefore the number of APs and RPs must be set. The determination of the optimal number for these parameters is called the calibration of the method. Note that what is tested in the calibration phase is not the particular classification process but the overall method performance under a particular selection of AP and RP numbers. A good AP–RP number combination would be attained if the particular configuration of the method has good predictive properties regarding the obtained precipitation projections, thus we test whether the method works or not as a whole. The calibration process will be presented and discussed deeply in next section.

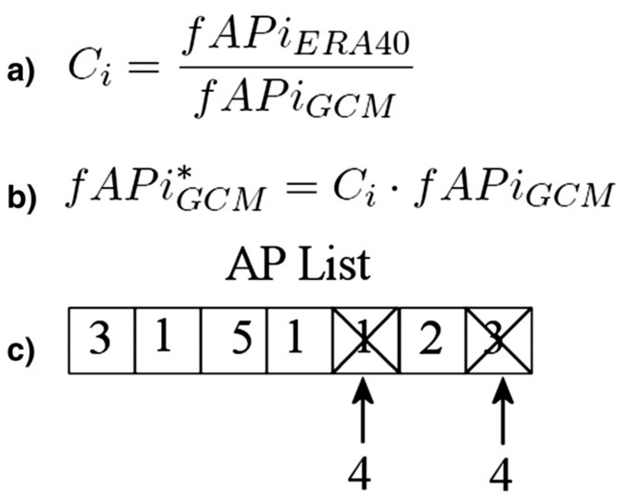

Fig. 7. AP frequency bias-correction schematic. a) Compensation coefficients are calculated from the training period as the comparison between ERA40 and GCM AP absolute frequencies. b) Coefficients are used in the prediction phase to obtain the unbiased GCM AP absolute frequencies. c) Days from AP excess classes are eliminated randomly and substituted for APs from deficient classes.

Owing to the different isobaric levels involved in the classification of atmospheric circulations, standardization is applied on the input variables in order to prevent dominance in the analysis of the 500 hPa geopotential, of larger magnitude and variability than at 850 hPa. Standardization is made on each day by subtracting the geographical mean of the day from the field and dividing the resulting spatial anomalies by the geographical standard deviation. The result is a spatial pattern at both levels without any information about the intensity of the lows, highs, troughs and ridges embedded in the circulation. The same type of standardization is applied for daily precipitation in coherence with the idea of classifying in base of the rainfall localization only. The magnitude of both atmospheric and rainfall perturbations is important for the final result, but this magnitude is used in a different step of the method.

It should be noted that since k-means algorithm is unable to handle days without precipitation, these are left out of the classification process and are incorporated afterwards as an additional category or cluster with its centroid obviously located at the zero point. Also, Principal Component Analysis (PCA) is carried out for atmospheric data on the one hand and for precipitation data (Benestad, 1999) on the other hand prior to applying the k-means classification method in order to identify directions that maximize variance. Requiring 95% of explained variance from PCA allows the reduction of the dimensionality from 70 to only 11 axes (Fig. 2) for atmospheric circulation data, and from 1145 to 789 axes for daily precipitation, allowing the classification to run in both cases with a reasonable computational effort.

Once atmospheric circulation and precipitation-structures are classified, these are related through a conditional probability matrix (M):

$$M = \begin{pmatrix} p(\mathrm{RP1}|\mathrm{AP1}) & p(\mathrm{RP2}|\mathrm{AP1}) & \dots & p(\mathrm{RPN}|\mathrm{AP1}) \\ p(\mathrm{RP1}|\mathrm{AP2}) & p(\mathrm{RP2}|\mathrm{AP2}) & \dots & p(\mathrm{RPN}|\mathrm{AP2}) \\ \vdots & \vdots & \ddots & \vdots \\ p(\mathrm{RP1}|\mathrm{APM}) & p(\mathrm{RP2}|\mathrm{APM}) & \dots & p(\mathrm{RPN}|\mathrm{APM}) \end{pmatrix}. \qquad (1)$$

Each M matrix cell represents the probability to find a RP given a known AP and is built from the day by day relationship between APs and RPs in the training data period. A real example is depicted in Fig. 4 and Table 2, corresponding to the 1961–1990 period with 9 RPs and 18 APs. Observe how high geopotentials over the domain correspond to a situation of scattered or almost no rain whereas lows are associated to intense and localized rainfalls in neighbor zones but, on the other hand, every AP has a significant chance of not leading to any rain. An unstable atmospheric situation can lead to intense and localized precipitation but it is not assured. At the same time lows are associated with a lower chance of a dry day than highs. These results are physically consistent and arise naturally from the classification and matrix building mechanism.

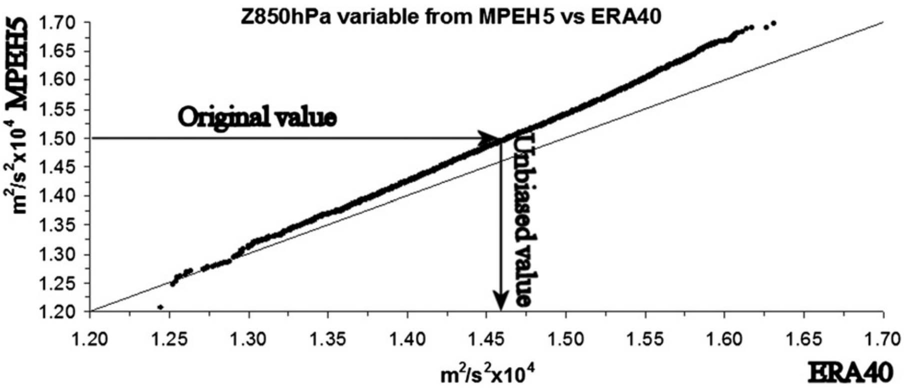

Fig. 8. Example of the quantile–quantile magnitude adjustment. A magnitude value from prediction period is searched in the GCM training data. By means of a quantile–quantile mapping from GCM to ERA40 an unbiased value is found.

Therefore M contains all the information about the causality relationship between atmospheric circulation types and precipitation distributions. This relationship is expected not to change, at least in a significant way, during the century. This is our interpretation of the stationarity hypothesis. Statistical methods are based on the assumption of a same behavior of the causal atmospheric mechanisms in the future, and here we have interpreted this hypothesis as the constancy of the conditional probability matrix in time. Observe in Fig. 3 for a selected AP–RP relationship how this hypothesis seems to be maintained in the present time analyzed data.

With Eq. (1) and the future daily atmospheric circulations also classified in terms of APs a prediction can be carried out. Naturally it is necessary that future circulations are classified on the same AP clusters found for the present climate. This classification is done by analogy: each circulation is classified in the same cluster as its most similar atmospheric state of the present time. Similarity here is defined as the Euclidean distance in the n-dimensional space mentioned above.

Knowing the AP of each future day a RP category is assigned to this day according to the discrete probability distribution contained in M matrix rows. This is done with the generation of nonuniform random numbers distributed according to the corresponding Probability Density Function (PDF). As each AP is more related to certain RPs and AP frequencies change with time, RP frequencies will also change in time. This stochastic RP generation process is in effect a weather generator. Fig. 5 illustrates the performance of this procedure when applied to two test periods. The frequency of RPs in the synthetic data is compared against the real occurrence and an agreement can be concluded (Kolmogorov–Smirnov test p-values for the comparison between real and synthetic distributions attain 73.58% and 98.58% in Fig. 5a and b, respectively. The null hypothesis is that both distributions are equal. The test would reject the null hypothesis for a significance level under 5%). A schematic representation of the method is displayed in Fig. 6.

An improvement of Sumner et al. (2003) method over other weather typing methods was its ability to correct the biases of the model in the frequency of atmospheric circulations. Future circulations are obtained from a GCM and classified as described. But runs of these models for the present time are also classified in order to check and correct these biases. Comparison of the ERA40 reanalysis AP absolute frequencies against GCM AP absolute frequencies gives information about the over- or under-representations of each model in terms of weather patterns that can be stored as coefficients:

$$C_i = \frac{fAPi_{ERA40}}{fAPi_{GCM}}. \quad (2)$$

This information is used over the predicted AP absolute frequencies to obtain a bias-corrected or compensated estimation of the future frequencies. Proportional excesses or deficits in APs according to Eq. (2) are corrected in a simple way by randomly eliminating days from the daily AP series from the exceeded stocks and replacing them by APs from the deficient stocks. This is done automatically by first selecting randomly an amount of days equal to the exceeded quantity and labeling them for deletion. Later, each of these days is replaced by APs from the deficient stock. The particular order in which these APs are inserted in the deleted positions is selected randomly. An outline of the process can be found in Fig. 7.

Finally, models are biased not only in AP frequencies but also in the overall magnitude of the fields. (Although the magnitude of the fields has not yet been used, it will be important in the next section). Therefore a quantile–quantile adjustment is applied on the spatial average of the predicted 850 hPa geopotential. That is, the most similar magnitude to the future GCM field is searched within the present period GCM run and its quantile level is mapped over the ERA40 statistics to find the unbiased or compensated magnitude (Fig. 8). The application of such type of quantile–quantile mapping transformations is a procedure that has been widely used for correcting biases in the simulated meteorological variables (e.g. Boé et al., 2007; Déqué, 2007; Amengual et al., 2012).

Table 3
Available populations for a 30 year period of training (see text).

Number of RPs	Number of APs	Categories	Days/category (approx.)	Points/RP (approx.)
4	8	32	342.2	361.3
5	10	50	219.0	289.0
6	12	72	152.1	240.8
7	14	98	111.7	206.4
8	16	128	85.5	180.6
9	18	162	67.6	160.6
10	20	200	54.8	144.5
11	22	242	45.2	131.4
12	24	288	38.0	120.4
13	26	338	32.4	111.2
14	28	392	27.9	103.2
15	30	450	24.3	96.3
16	32	512	21.4	90.3
17	34	578	18.9	85.0
18	36	648	16.9	80.3
19	38	722	15.2	76.1
20	40	800	13.7	72.3
21	42	882	12.4	68.8
22	44	968	11.3	65.7
23	46	1058	10.3	62.8
24	48	1152	9.5	60.2

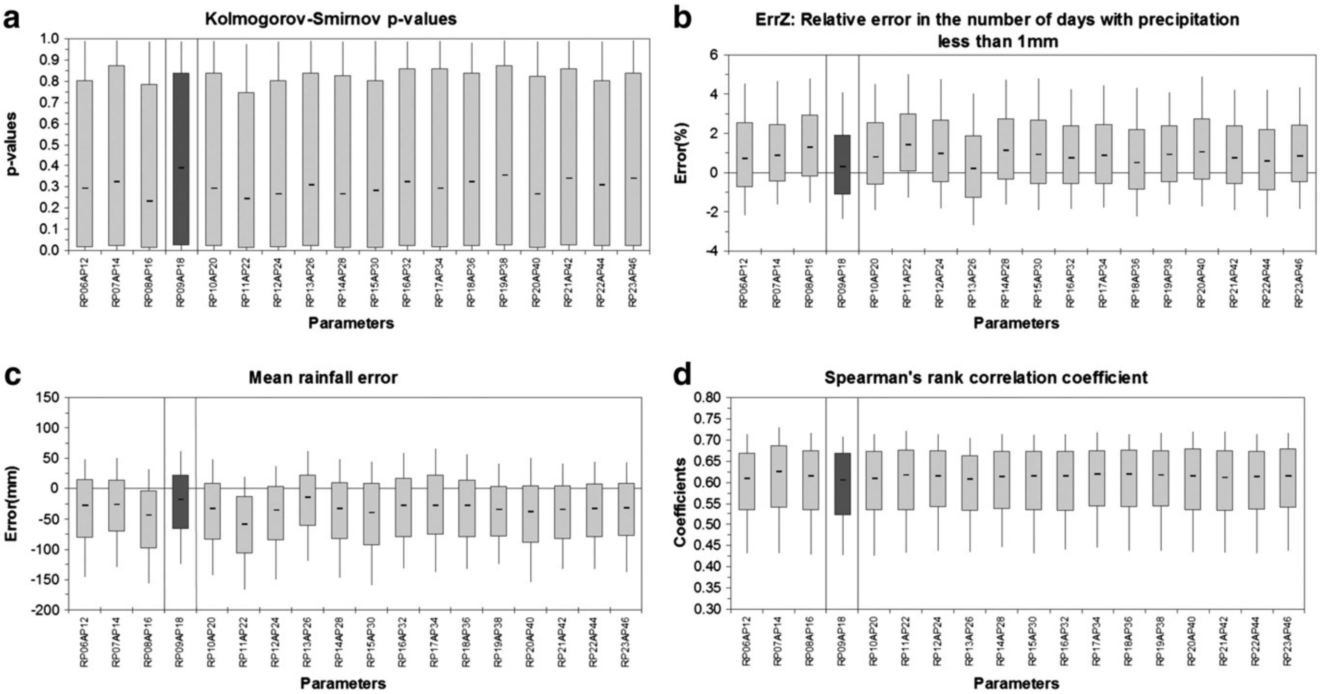

Fig. 9. a) Kolmogorov–Smirnov p-values, b) Relative error in the number of days with precipitation under 1 mm ErrZ, c) Mean rainfall error and d) Spearman's rank correlation coefficient. The training period used is 1961–1990 and the prediction period 1991–1999. Number of APs is chosen as twice the number of RPs. 9 RPs and 18 APs are selected as the best configuration.

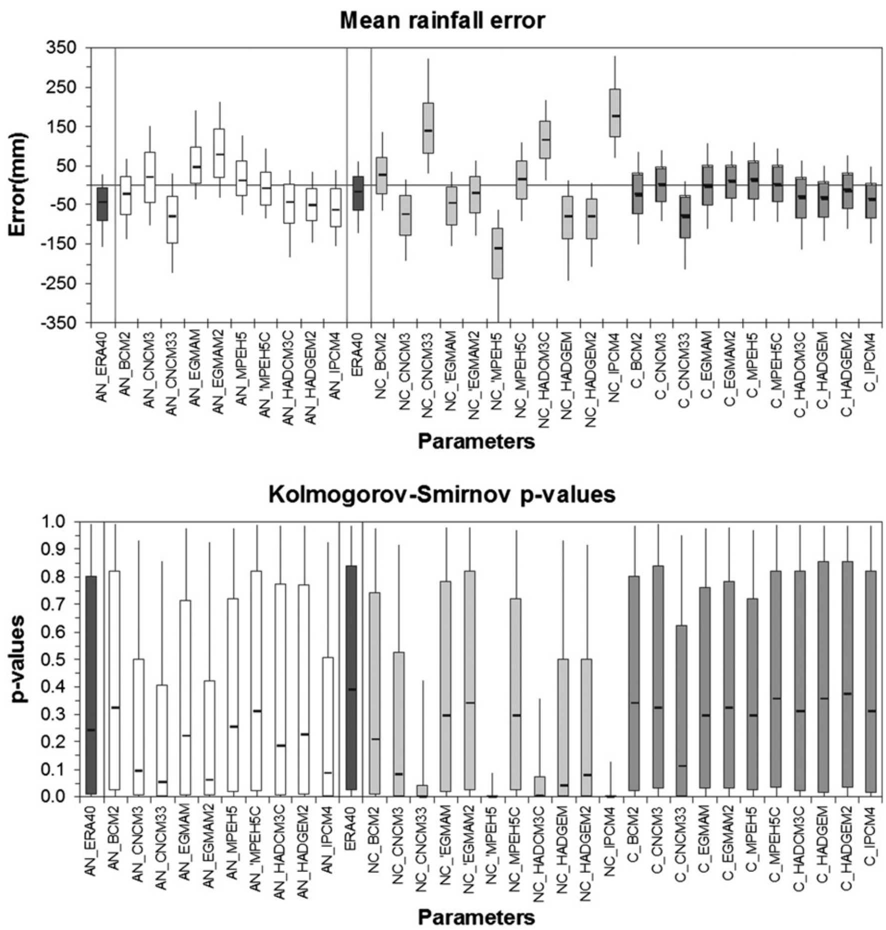

Fig. 10. Mean rainfall error and Kolmogorov–Smirnov p values after applying the downscaling method to different GCMs. The training period used is 1961–1990 and the prediction period 1991–1999. The chosen configuration is the best one from the calibration phase: 9 RPs and 18 APs. Compensated and uncompensated results are compared (C and NC prefix respectively) and also with the results obtained from an analog method (AN prefix). For comparison, the statistics in perfect prog (i.e. using ERA40) are included as dark bars.

2.3. Rainfall map selection

To this point only the rainfall spatial distribution (i.e. RP) has been determined for each future day, without regard to the magnitude of the field. To generate a complete daily rainfall map a present day pertaining to that RP is chosen. An advantage of this strategy is that by identifying a future realization with a whole daily map the spatial coherence of the generated rainfall field is ensured. However, the selection of the daily map should not be completely random because changes on future atmospheric temperature and thus in the overall magnitude of the geopotential field offer motivations to expect that rainfall magnitude probability will not remain constant in the future. The rainfall map selected is that belonging to a present day pertaining to the same RP and with the closest 850 hPa geopotential spatial average to the future day. Note that the spatial pattern of the atmospheric circulation is not relevant at this point because it has already been considered when the AP category of the day has been determined in a previous step. Therefore the magnitude of the 850 hPa background height field is used to reduce the selection of a daily rainfall map to the most similar day from the training period.

3. Calibration

The downscaling methodology is dependent on two subjective choices, number of APs and RPs. A calibration of the algorithm must be thus achieved before producing the rainfall projections. As a general rule we consider a range of different RP sets, setting the AP number as twice the RP number. This strategy is justified by the practical need of using more AP categories than RP categories because no rain events combine into a single RP class but the number of responsible synoptic circulation patterns may be very diverse. A simple analysis over the resulting statistical populations (Table 3) guides the selection of a reasonable range of parameters suitable to perform the calibration. The conditional probability matrix has a dimension given by the RP number N times the AP number M. The relation between the total number of days included in the training data set and the number of matrix cells leads to a rough estimate of the statistical significance of these conditional probabilities, which should be calculated using a sufficient population of days. Higher ratios of AP number versus RP number have been tested but show no better results while they have the potential to lead to matrix cells poorly represented in statistical terms. On the other hand the

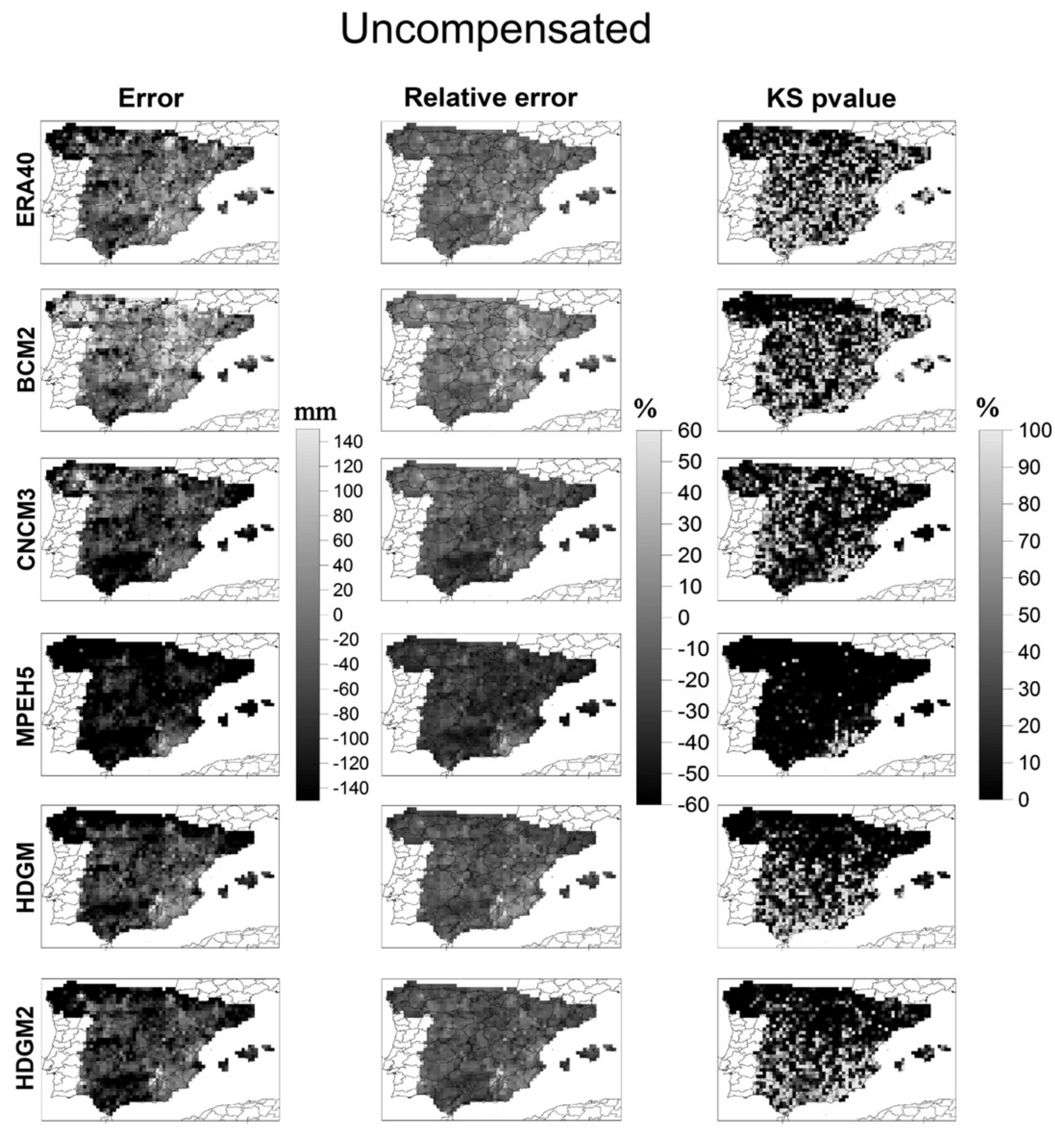

Fig. 11. As in Fig. 10 but in terms of the spatial maps of mean rainfall error and Kolmogorov–Smirnov p-values (uncompensated results).

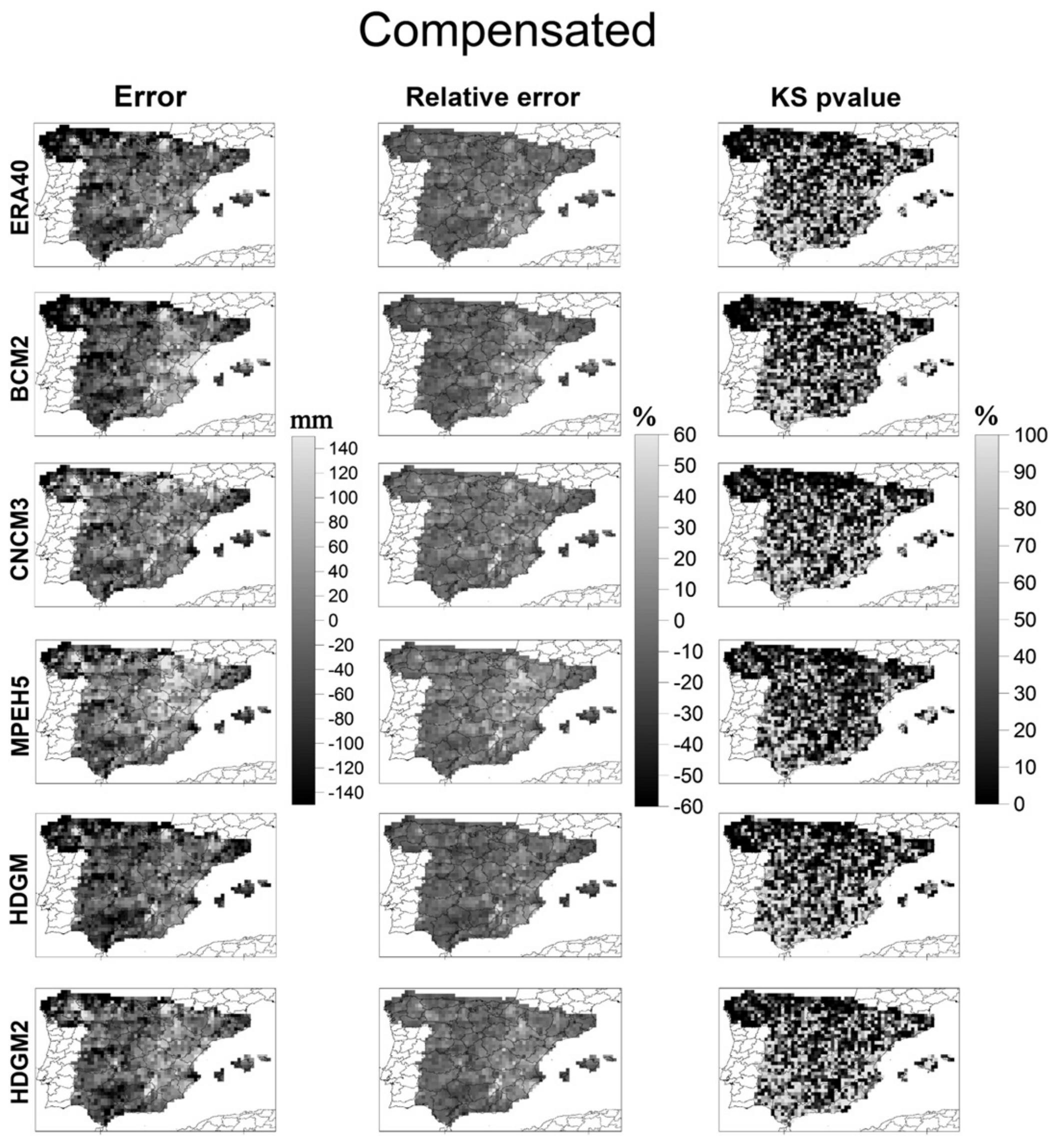

Fig. 11. (*Continued*) As in Fig. 10 but in terms of the spatial maps of mean rainfall error and Kolmogorov-Smirnov p-values (compensated results).

relation between the number of Spain02 grid points and the number of rain patterns is informative about how well represented the different RPs are. If we take 250 points as the typical size of the major hydrographic basins of Spain, RPs with dimensions larger than this value would be clearly underrepresenting the spatial variability of rainfalls. A range between 6 and 20 RPs has been considered reasonable to perform the calibration.

The method is trained using the period 1961–1990 and tested for the period 1991–1999. Daily rainfall series are generated for this period and a comparison between synthetic and real series is done. This calibration is performed in perfect prog, that is, training and predicting with ERA40 reanalysis data. Four statistics have been used: three measures of the quality of the synthetic distribution (Kolmogorov–Smirnov p-values, Spearman's rank correlation coefficient and relative error in dry days) and mean rainfall error. The combination of these four types of measures provides a complete picture of the goodness of the predicted data. Panels in Fig. 9 show the results for each combination of RPs and APs as boxplots. These boxplots are constructed from the statistical indices obtained for the predicted series at each grid point of the map: the central point at the boxplot is the median of the map for the corresponding statistic and the limits of the box are the 25 and 75 percentiles; the whisker extremes are the 10 and 90 percentiles.

The Kolmogorov–Smirnov test (Fig. 9a) is performed over the predicted rainfall distribution with the real rainfall as the reference distribution. The analysis is carried out over the obtained p-values to evaluate the confidence in the similarity between the distributions. The rejection threshold is set at 5%. Only a small fraction of the grid points of the map fall under this value. When the map is evaluated as a whole the overall behavior of the method is satisfactory. A complementary statistic to the Kolmogorov–Smirnov test is the relative error in the number of days with precipitation less than 1 mm (here abbreviated ErrZ; Fig. 9b). Kolmogorov–Smirnov test yields a score regarding the whole daily series distribution without distinguishing if a drop in confidence is due to the over or underrepresentation in the series of intense, light or no precipitation days. Intense precipitation events are rare and harder to predict owing to the lack of statistical population of extreme events. Days with extreme precipitation are influential on the mean annual rainfall map, but since they are rare, its weight on the annual rainfall becomes less important than the weight of days with light or no rain. In effect, a strong correspondence is shown between ErrZ and the mean rainfall error (Fig. 9c) pointing out that a correct prediction of the number of under 1 mm rain days is most relevant to the mean map than an accurate statistic of intense events. This high correspondence makes one of the two statistics enough

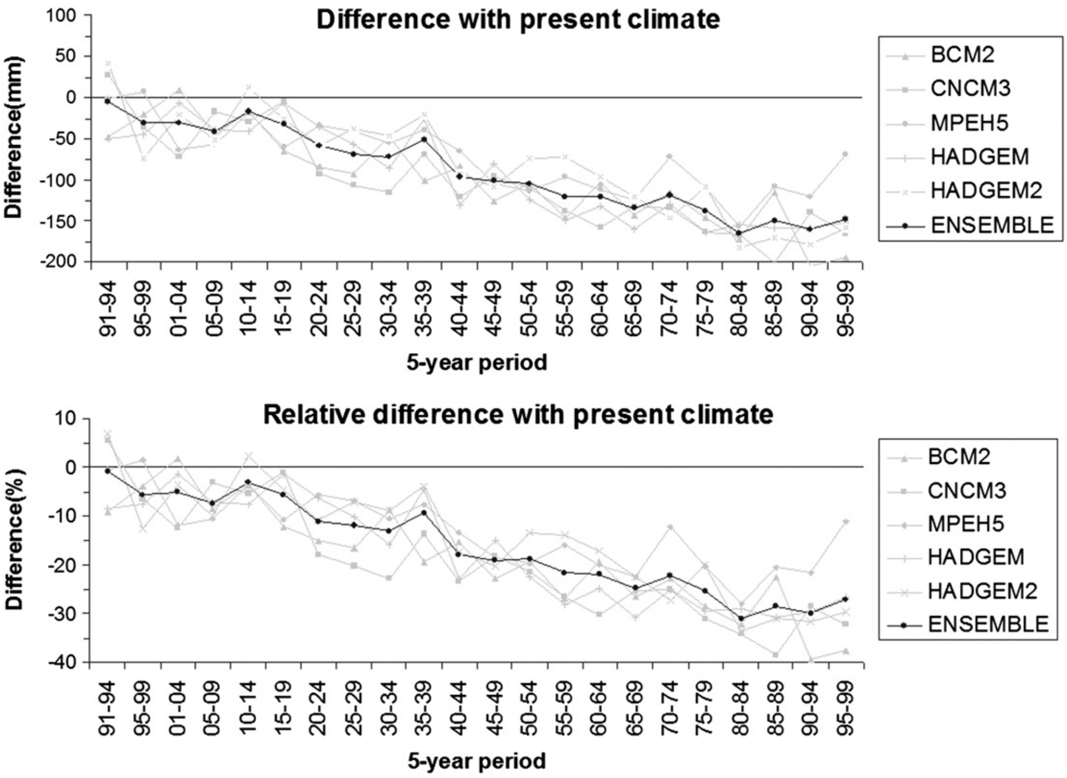

Fig. 12. Summary of the comparison between the A1B scenario and present climate mean rainfall. Plotted is the median of the change (upper panel) and of the relative change (lower panel) between the mean maps corresponding to 5-year periods of the 21st century and present climate mean map. Each curve in gray is from a projection using a different circulation model. In black the result for the ensemble mean is shown.

for our purposes and the mean rainfall error (Mme) is more common in literature (Gutiérrez et al., 2004; Wilks, 2006).

Correlation is measured with the Spearman's rank correlation coefficient (Fig. 9d). The median of the boxplot is around 0.6, a moderate value. That means that the method is capable of discriminating between wet and dry seasons and also identifying correctly the fraction of rainy to dry days, enabling a seasonal climate analysis.

The best overall result is found at 9 RPs and 18 APs and this will be our selected configuration of the method for the rest of the study. Nevertheless, there are no large differences between high and low RP/AP combinations, probably because the resolved spatial scale of the atmospheric circulation and rainfall distribution in the used databases lacks mesoscale information.

4. Validation

Calibration has been developed in perfect prog with ERA40 reanalysis data to obtain the proper RP/AP configuration. Before making any future projection the workability of the method with GCM data must be tested and validated. As for calibration, the method is trained with the period 1961–1990 and tested in the period 1991–1999, this time with each GCM as atmospheric circulation source. The same statistical indices were calculated and can be found in Figs. 10 and 11 in boxplot and map forms, respectively. Validation is performed in two modes: compensated and uncompensated. Uncompensated skips any compensation steps of the method (recall Section 2 and the compensation procedure summarized in Fig. 7); the comparison between both

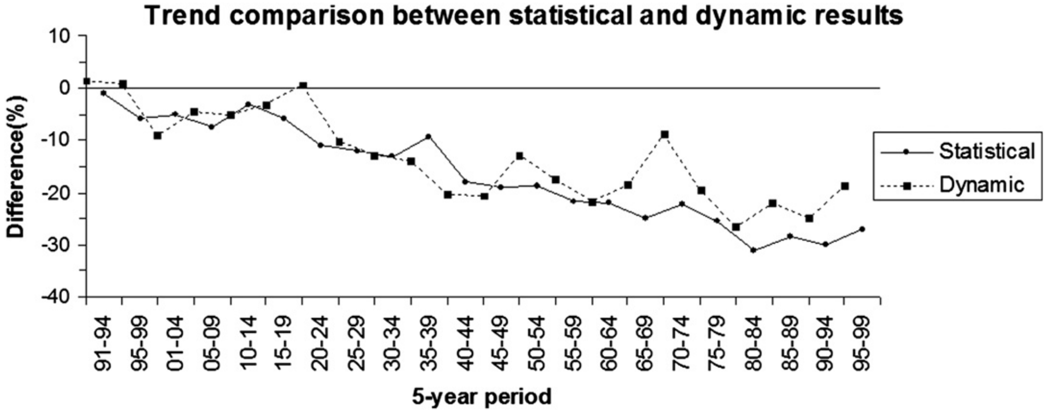

Fig. 13. As in Fig. 12, but showing a comparison for the relative change between the ensemble mean obtained with the statistical projection method and the ensemble mean obtained directly from the Global Climate Models. Note we are comparing results from maps with a very different spatial resolution, thus the comparison is merely orientative.

approaches is useful to point out the great importance of correcting the biases of the models in AP frequency and field magnitude. Compensation is revealed as essential to produce an accurate rainfall prediction as noted in the great improvement of the distribution of p values and the mean rainfall for all the source models. Even poorly behaved models such as MPEH5, with almost all its points under the confidence level, become useful for prediction if compensated, yielding similar results to the rest of source models. In summary, the method seems to be validated because the results obtained for the test period using the GCMs as input data are generally similar to the perfect prog predictions.

Additionally, a comparison with the analog method (Zorita and von Storch, 1999) is provided (Fig. 10). The analog method was previously tested with different configurations and predictors under the same training and prediction periods. A configuration of the analog method with mean sea level pressure and temperature at 850 hPa as predictors arose as the best choice. To make the comparison in fair conditions the biases of the GCM variables were first corrected on a monthly basis prior to feed the algorithm. Note the robustness of the proposed methodology in comparison with the analog method, offering similar results regardless of the GCM model used as source of the atmospheric circulation. The analog method is more sensitive to the choice of predictors and to the different models because it is more dependent on local features of the meteorological fields.

5. Precipitation projections

In this section our validated method is applied to achieve the 21st century precipitation projections for the period 2001–2099. Circulation input data is taken from five different GCMs under the most studied emission scenario: SRES-A1B. GCM selection is based on data availability although more models were considered in the validation phase for completeness and as a guide for future work. As for the calibration and testing of the method in the last sections, it is trained for the period 1961–1990 and we will use the best configuration found, i.e. 9 RPs and 18 APs.

Although the future projection for each model is obtained in a single run, the data are analyzed in 5-year periods. This kind of analysis allows tracking of the changes all along the 21st century. Our specific interest is to determine the changes in precipitation in comparison to the present climate. Thus the mean rainfall of each 5-year period is compared against the present climate mean rainfall corresponding to the training period. Two different but related measures are analyzed, absolute change between rainfall maps and relative change with respect to the present climate. The spatial medians of these two measures are displayed as time series in Fig. 12 for the different GCM models and the ensemble mean. It is remarkable that the rainfall decreasing trend obtained in the statistical projections is consistent with the raw precipitation results given by the Global Climate Models (Fig. 13). Since the models' precipitation data are not used in the statistical prediction schemes, then this outcome is only a consequence of changes in the large-scale circulation in the global models.

Observe how precipitation decreases almost linearly in Peninsular Spain and the Balearic Islands throughout the 21st century. The loss in the map median reaches almost 30% in only one century (Fig. 12). That would imply a very high climatic impact on precipitation with great effects over ecosystems and society. The boxplot for the ensemble mean (Fig. 14) shows that at some points this annual precipitation loss reaches almost 40%. How much of this loss is due to changes in the

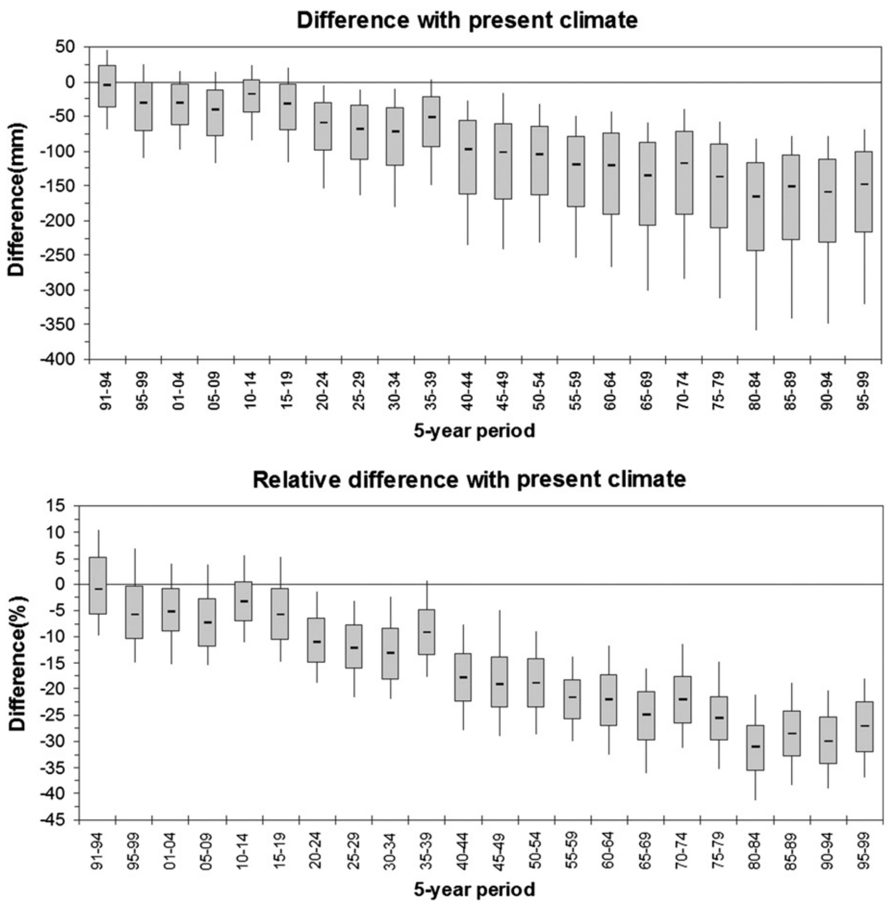

Fig. 14. Boxplot of the change and relative change between mean rainfall in future A1B scenario and present climate. Plotted is the geographical median of the change as a black horizontal line, box limits are 25 and 75 percentiles and the extremes of the whiskers are the 10 and 90 percentiles.

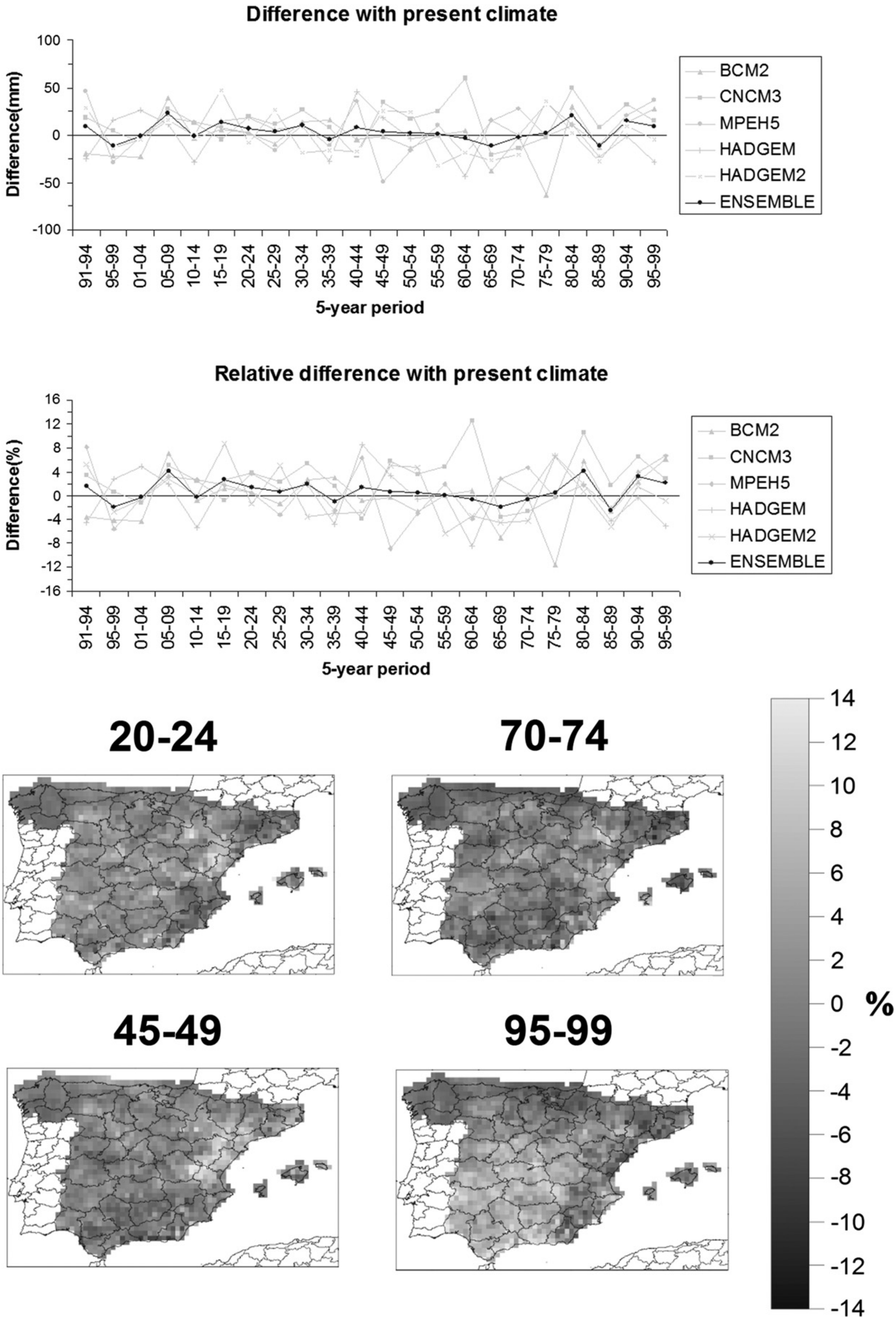

Fig. 15. As in Fig. 12 but from the application of the method with a random selection of future day rainfall maps, without attending to changes in magnitude of atmospheric circulation (see text). A depiction of the relative changes as spatial maps for four selected 5-year periods is included in the lower panel.

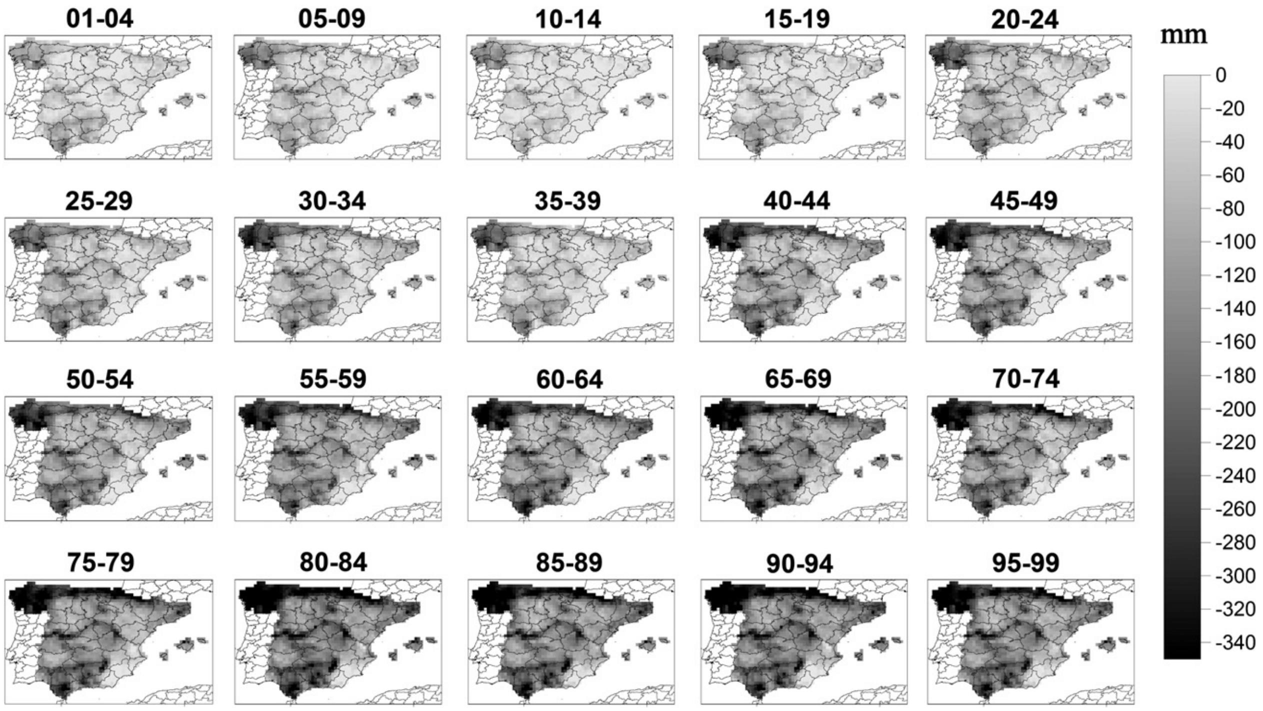

Fig. 16. Maps of ensemble mean absolute change in annual rainfall between each 5-year period of the 21st century and present climate (1961–1990).

frequency of atmospheric circulation structures and how much to changes in their magnitude? These two roles can be evaluated: once the type of RP assigned to each future day is determined, if the final daily map is selected randomly and ignoring magnitude changes on circulation (recall Section 2.3), no trend is observed in the geographical median of the rainfall in Peninsular Spain and the Balearic Islands (see Fig. 15). However, that doesn't imply that there are no regional changes; as can be seen in the same figure there is a redistribution of rainfall. Note in particular the slight increase of precipitation in South Spain. From this result it is learned that the change in magnitude of the patterns can overcome the effects of the changes in frequency. In other words, some patterns become more frequent thus more rain in certain regions could be expected but since they are less intense a final drying can occur; a clear example shown next is South Peninsular Spain. It is

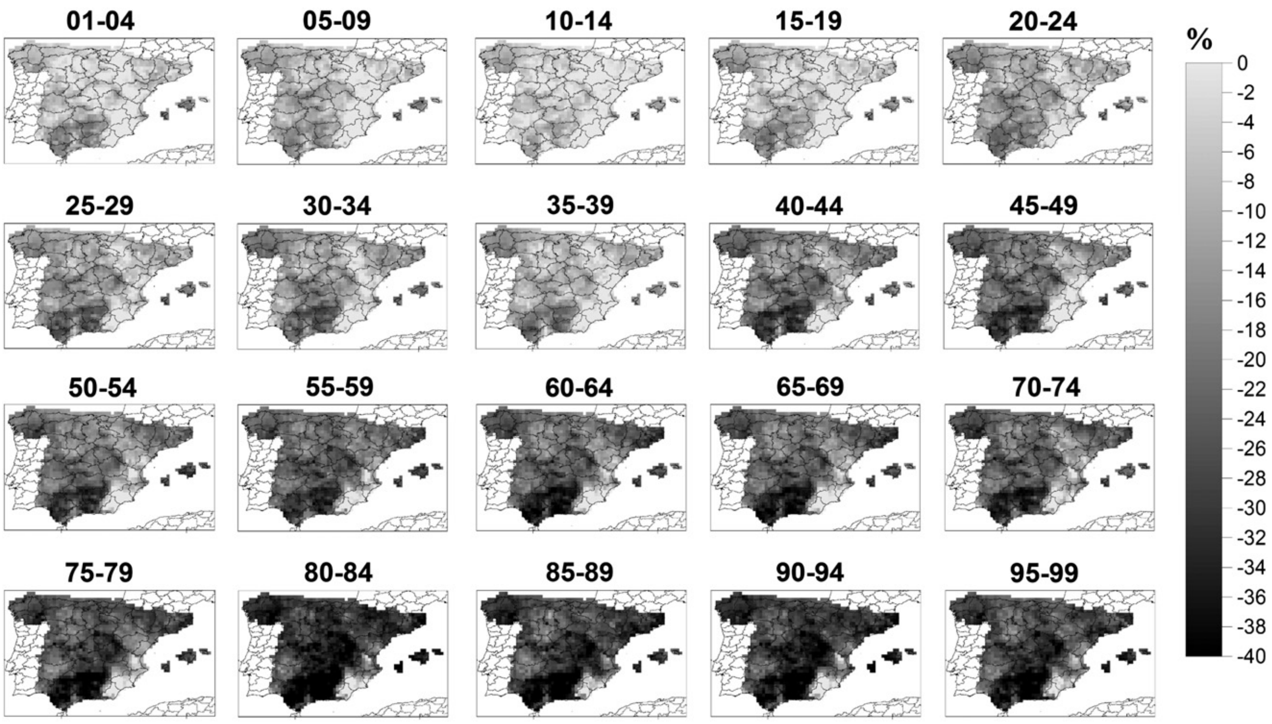

Fig. 17. As in Fig. 16 but for the relative change.

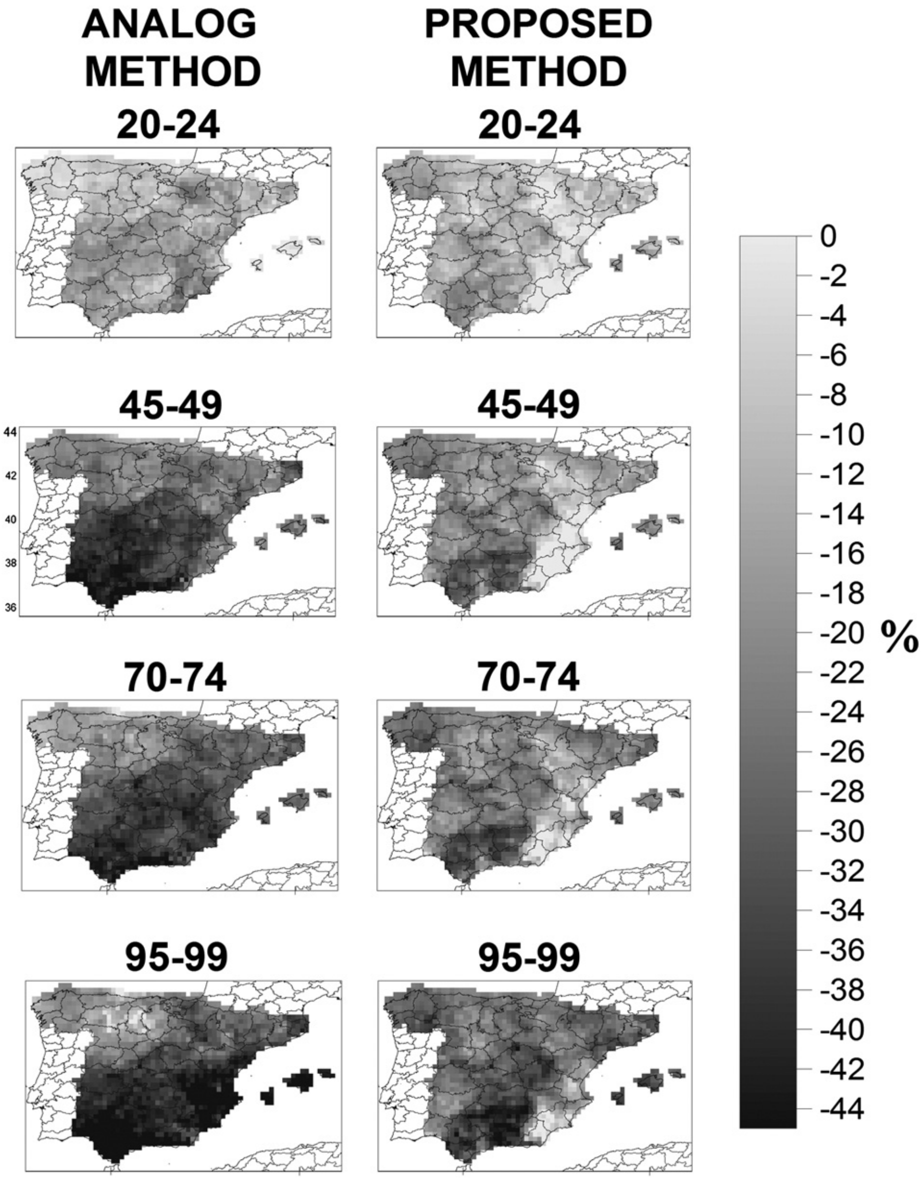

Fig. 18. Comparison between the ensemble-mean relative change in annual precipitation with respect to the present climate in the analog method and the proposed method. A representative set of 5-year periods from the 21st century is selected.

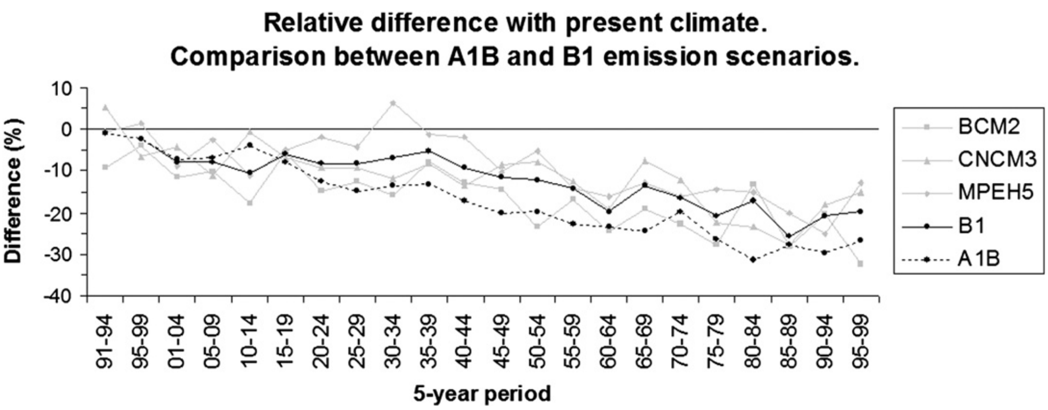

Fig. 19. Comparison between A1B and B1 emission scenarios. The relative changes with respect to the present climate for each model projection in B1 emission scenario are depicted in gray and give an idea of the spread of the results. The black line indicates the B1 ensemble mean of the three available models. The A1B emission scenario ensemble mean from the same three models is represented as dotted black line.

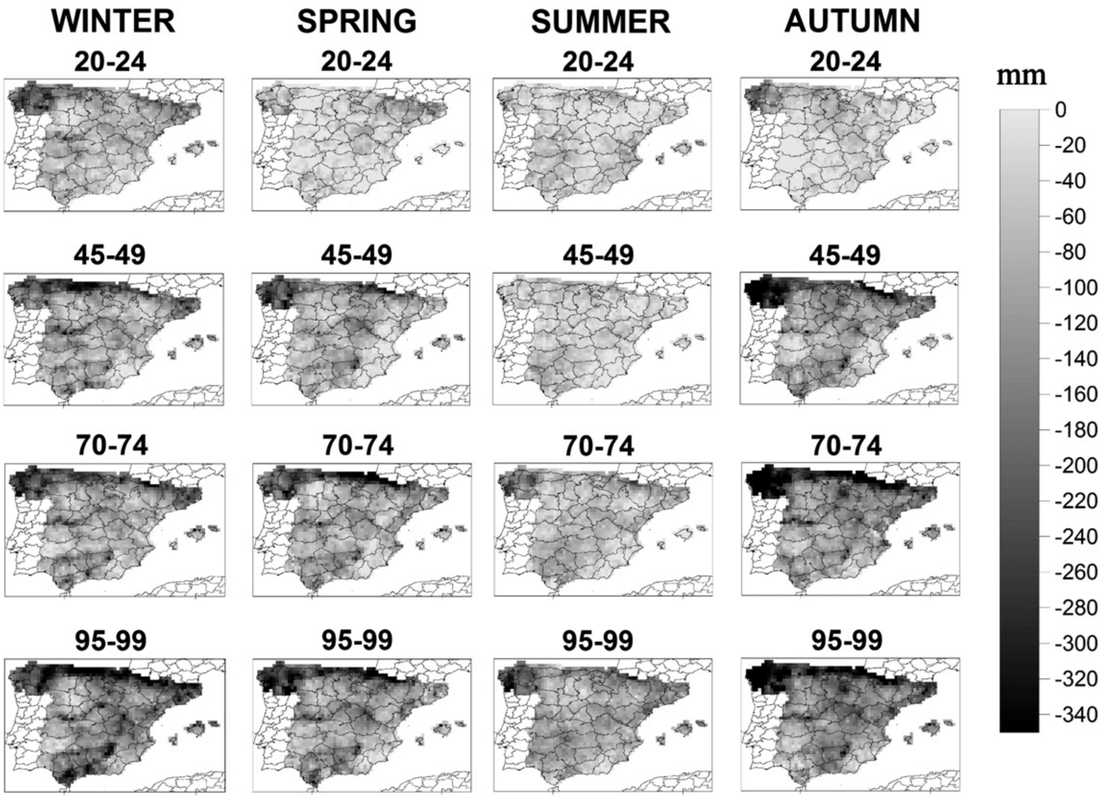

Fig. 20. Maps of ensemble mean absolute change in seasonal precipitation with respect to the present climate for the 21st century in the A1B scenario.

necessary to take into account both effects for an accurate prediction even if they have opposite roles in a certain region. Also note that circulation intensity changes may be different between atmospheric patterns.

Time series and boxplots are very useful to deal with trends but spatial maps are necessary to study geographical distributions. Figs. 16 and 17 show spatial maps of both measures (absolute change

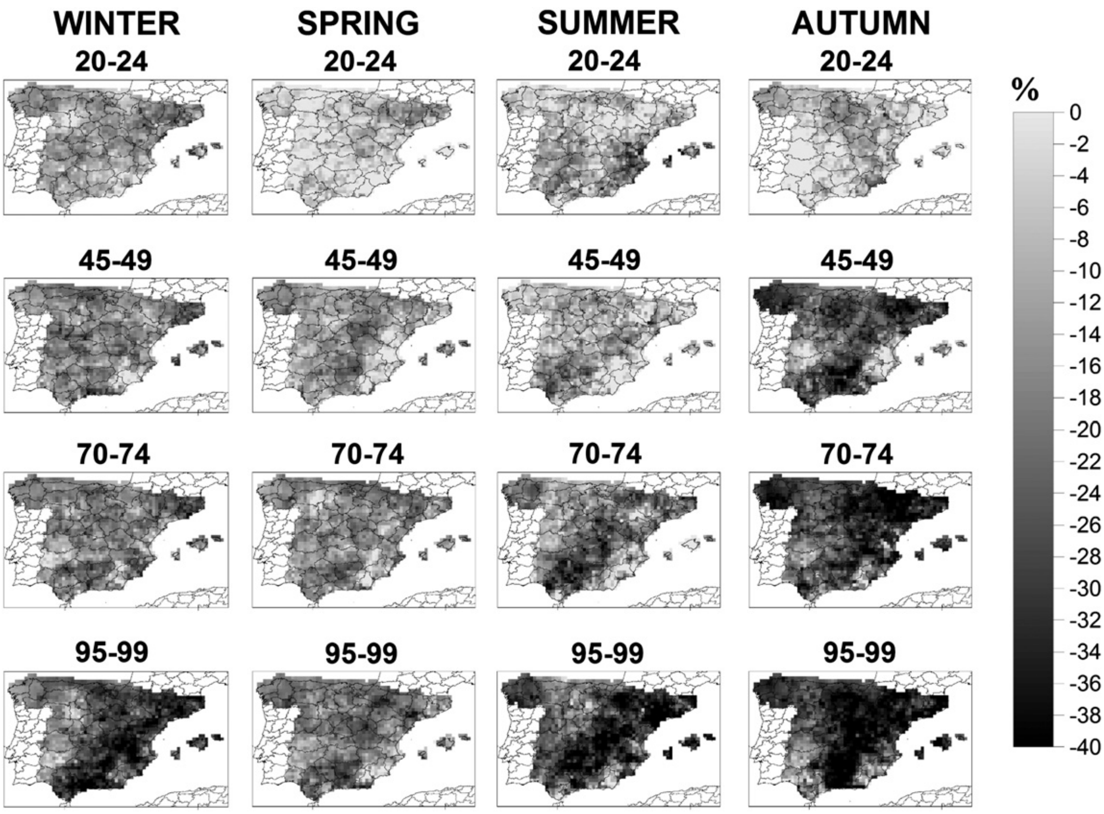

Fig. 21. As in Fig. 20 but for the relative change in seasonal precipitation.

and relative change with respect to the present climate) for each 5-year period (note that the first period comprises 4 years instead of five). As shown, Peninsular Spain becomes drier as the century progresses, being the first affected regions the South and West of the Iberian Peninsula. A few Mediterranean regions would remain relatively unaffected until the last decades of the century. At the end of the period almost all Peninsular Spain and the Balearic Islands would have its precipitation reduced around 30%. Ebro and Duero basins lie under the mean with a rainfall drop of around 20% and Segura basin around 10%. A novel result of our method is the prediction of an early climatic change impact in all western Peninsular Spain including northern regions such as Galicia. This result is supported by recent observations (Hoerling et al., 2012) and has been previously unseen by other methods such as the analog method used as reference in this work. In the comparison displayed in Fig. 18 it is shown that the analog method projects a rainfall reduction from South to North continuous in time. The aforementioned redistribution of rainfall in the present methodology results in western regions and even northern ones to be affected from the very beginning of the century.

A comparison of the previous results with the B1 emission scenario is shown in Fig. 19. A less emissive scenario would result in a relative stabilization of the precipitation amount during the first 40 years of the century. However the negative trends during the rest of the century are similar, resulting in a net effect of about 10% more precipitation in B1 scenario than in A1B scenario at the end of the period. The change from a stationary situation to a decreasing trend happens very quickly in B1 scenario without practically no transition phase between them.

Figs. 20 and 21 display the expected changes in seasonal precipitation for A1B scenario. Observe that the two most widely affected seasons by climate change in absolute terms are winter and autumn, but the changes in autumn are more noticeable in the early 21st century. Being summer the less rainy season, the projected loss of precipitation in this period of the year is comparable to winter and autumn in relative terms. The greatest decrease in precipitation amount at the end of the century is obtained in the northern Peninsular Spain but the largest relative change compared to the present climate occurs in Mediterranean regions and the center of the peninsula. In relative terms, drier regions become even more dry than wet zones. Spring seems to be the less affected season but at the end of the century a reduction of about 20% of precipitation is experienced in a more or less uniform way across Peninsular Spain.

6. Conclusions and further work

A novel use of two well known strategies, weather typing and weather generation, was made in this work to produce a new downscaling method. This method has been calibrated to provide future rainfall projections over Peninsular Spain and the Balearic Islands and its performance has been validated over a present period using 11 different GCMs as source of the atmospheric circulation information. The downscaling method exhibits a wider application in comparison with the analog method. This characteristic is attributable to two reasons: first, to the fact that the method only needs 18 AP classes to properly represent the different atmospheric patterns over the domain of interest, thus the method relies on the identification of the general structure of the atmospheric flow and not on its details; and second, to the use of compensated daily circulation series in the statistical weather generation that permits to minimize the negative effects of the biases inherent to the input atmospheric data. Compensation is not a new idea but this work has deepened in the concept in comparison with previous works in order to translate its benefits directly to daily time series of atmospheric circulation.

The specific application of the method over Peninsular Spain and the Balearic Islands points out great effects in this region throughout the 21st century. Around 30% decreases in annual rainfall are expected on average for the A1B emission scenario. Projected precipitation loss is not uniform in time and across Peninsular Spain. The present method shows that the changes will be noticeable first on west Peninsular Spain at the beginning of the century and by the end of the century the entire Iberian Peninsula will be largely affected. This projection is different from the analog downscaling method that just shows a South to North Peninsular Spain loss of precipitation in time. The greatest decreases in precipitation amount in absolute terms is found in the North of Spain, but relative changes will be more uniform. The present work also projects that around 10% of this precipitation loss can be saved in a less emissive scenario like B1. Seasonally, the drying process will affect all periods of the year although precipitation decreases in autumn will be already noticeable during the early 21st century.

Finally, we have not yet reached the full applicability of the method in this paper. The present GCM selection is based on data availability but a larger collection of models and emission scenarios will be considered for future work. Also, other variables of great practical interest in addition to precipitation are suitable to receive the same type of statistical treatment for the generation of future projections, in particular the daily maximum and minimum temperatures. These climatic datasets will form the basis of future interdisciplinary studies aimed at assessing the impacts of global warming on strategic natural and socioeconomic sectors of Spain.

Acknowledgments

The authors thank AEMET and University of Cantabria for providing the data used in this work (Spain02 dataset). This work was supported by esTcena project (Exp. 200800050084078), a strategic action from Plan Nacional de I+D+i 2008–2011 funded by Spanish Ministry of Medio Ambiente y Medio Rural y Marino.

References

Amengual, A., Homar, V., Romero, R., Alonso, S., Ramis, C., 2012. A statistical adjustment of regional climate model outputs to local scales: application to Platja de Palma, Spain. Journal of Climate 25, 935–957.
Anderberg, M.R., 1973. Cluster analysis for applications. Probability and Mathematical Statistics, vol. 19. Academic Press, New York.
Benestad, R.E., 1999. S-mode and T-mode EOFs from GCM modeller's perspective. Notes on Linear Algebra, vol. 24/99. Klima, DNMI, PO Box 43 Blindern, 0313 Oslo, Norway.
Benestad, R.E., Hanssen-Bauer, I., Chen, D., 2008. Empirical-statistical Downscaling. World Scientific, 27 Warren Street, Suite 401–402, Hackensack, NJ 07601.
Boé, J., Terray, L., Habets, F., Martin, E., 2007. Statistical and dynamical downscaling of the Steine basin climate for hydrometeorological studies. International Journal of Climatology 27, 1643–1655.
Chen, J., Brissette, F.P., Leconte, R., 2010. A daily stochastic weather generator for preserving low-frequency of climate variability. Journal of Hidrology 3, 480–490.
Chou, C., Chen, C.A., Tan, P.H., Chen, K.T., 2012. Mechanisms for global warming impacts on precipitation frequency and intensity. Journal of Climate 25, 3291–3306.
Cofiño, A., Ancell, R., San-Martín, D., Herrera, S., Gutiérrez, J., Manzanas, R., 2010. Meteolab library. URL: http://www.meteo.unican.es/es/software/meteolab.
Dai, A., 2006. Mechanisms for global warming impacts on precipitation frequency and intensity. Journal of Climate 19, 4605–4630.
DelSole, T., Tippett, M.K., Shukla, J., 2011. A significant component of unforced multidecadal variability in the recent acceleration of global warming. Journal of Climate 24, 909–926.
Déqué, M., 2007. Frequency of precipitation and temperature extremes over France in an anthropogenic scenario: model results and statistical correction according to observed values. Global and Planetary Change 57, 16–26.
Duda, R.O., Hart, P.E., Stork, D.G., 2001. Pattern Classification. Wiley-Interscience, 605, Third Avenue, New York.
Durack, P.J., Wijffels, S.E., 2010. Fifty-year trends in global ocean salinities and their relationship to broad-scale warming. Journal of Climate 23, 4342–4362.
Fovell, R.G., Fovell, M.Y.C., 1993. Climate zones of the conterminous United States defined using cluster analysis. Journal of Climate Change 6, 2103–2135.
Fu, G., Charles, S.P., Kirshne, S., 2013. Daily rainfall projections from general circulation models with a downscaling nonhomogeneous hidden Markov model (NHMM) for south-eastern Australia. Hydrological Processes (in press).
Giorgi, F., Mearns, L., 1991. Approaches to the simulation of regional climate change: a review. Reviews of Geophysics 29, 191–216.
Gutiérrez, J.M., Cano, R., Cofiño, A.S., Sordo, C.M., 2004. Redes Probabilísticas y Neuronales en las Ciencias Atmosféricas. Monografías del Instituto Nacional de Meteorología, Centro de publicaciones de la Secretaría General Técnica del Ministerio de Medio Ambiente, Madrid.
Harin, V.V., Zwiers, F.W., Zhang, X., Hegerl, G.C., 2007. Changes in temperature and precipitation extremes in the IPCC ensemble of global coupled model simulations. Journal of Climate 20, 1419–1444.

Held, I.M., 1993. Large-scale dynamics and globar warming. Bulletin of the American Meteorological Society 74, 228–241.
Herrera, S., Gutiérrez, J.M., Ancell, R., Pons, M., Frías, M.D., Fernández, J., 2010. Development and analysis of a 50 year high-resolution daily gridded precipitation dataset over Spain (Spain02). International Journal of Climatology 32, 74–85.
Hoerling, M., Eischeid, J., Perlwitz, J., Quan, X., Zhang, T., Pegion, P., 2012. On the increased frequency of Mediterranean drought. Journal of Climate 25, 2146–2161.
Jeong, D., St-Hilaire, A., Ouarda, T.B.M.J., Gachon, P., 2011. Multisite statistical downscaling model for daily precipitation combined with multivariate multiple linear regression and stochastic weather generation. Climatic Change 114, 567–591.
Nakicenovic, N., Alcamo, J., Davis, G., de Vries, B., Fenhann, J., Gaffin, S., Gregory, K., Grubler, A., Jung, T.Y., Kram, T., Rovere, E.L.L., Michaelis, L., Mori, S., Morita, T., Pepper, W., Pitcher, H.M., Price, L., Riahi, K., Roehrl, A., Rogner, H.H., Sankovski, A., Schlesinger, M., Shukla, P., Smith, S.J., Swart, R., van Rooijen, S., Victor, Nadejda, Dadi, Z., 2000. Emissions scenarios. A Special Report of Working Group III of the Intergovernmental Panel on Climate Change.Cambridge University Press, 40 West 20th Street, New York.
Ribalaygua, J., Borén, R., 1995. Clasificación de patrones espaciales de precipitación diaria sobre la España peninsular y Baleárica. Informe n 3 del servicio de análisis e investigación del clima.INM, Madrid.
Romero, R., Ramis, C., Guijarro, J.A., 1999a. Daily rainfall patterns in the Spanish Mediterranean area: an objective classification. International Journal of Climatology 19, 95–112.
Romero, R., Sumner, G., Ramis, C., Genovés, A., 1999b. A classification of the atmospheric circulation patterns producing significant daily rainfall in the Spanish Mediterranean area. International Journal of Climatology 19, 1027–1040.
Romps, D.M., 2011. Response of tropical precipitation to global warming. Journal of the Atmospheric Sciences 68, 123–138.
Solomon, S., Qin, D., Manning, M., Chen, Z., Marquis, M., Averyt, K., Tignor, M., Miller, H., 2007. IPCC (2007) Climate Change 2007: The Physical Science Basis. Cambridge university press, 40 West 20th Street, New York.
Sørup, H.J.D., Madsen, H., Arnbjerg-Nielsen, K., 2012. Descriptive and predictive evaluation of high resolution Markov chain precipitation models. Hydrological Processes 23, 623–635.
Sumner, G.N., Romero, R., Homar, V., Ramis, C., Alonso, S., Zorita, E., 2003. An estimate of the effects of climate change on the rainfall of Mediterranean Spain by the late of twenty first century. Climate Dynamics 20, 789–805.
Uppala, S.M., Kållberg, P., Simmons, A., Andrae, U., Bechtold, V.D.C., Fiorino, M., Gibson, J.K., Haseler, J., Hernandez, A., Kelly, G.A., Li, X., Onogi, K., Saarinen, S., Sokka, N., Allan, R.P., Andersson, E., Arpe, K., Balmaseda, M.A., Beljaars, A.C.M., Berg, L.V.D., Bidlot, J., Bormann, N., Caires, S., Chevallier, F., Dethof, A., Dragosavac, M., Fisher, M., Fuentes, M., S., Hólm, E., Hoskins, B.J., Isaksen, L., Janssen, P.A.E.M., Jenne, R., McNally, A.P., Mahfouf, J.F., Morcrette, J.J., Rayner, N.A., Saunders, R.W., Simon, P., Sterl, A., Trenberth, K.E., Untch, A., Vasiljevic, D., Viterbo, P., Woollen, J., 2005. The ERA-40 re-analysis. Quarterly Journal of the Royal Meteorological Society 131, 2961–3012.
Wilks, D.S., 2006. Statistical methods in the atmospheric sciences: an introduction, Second edition. International Geophysics Series, vol. 91. Academic Press, 30 Corporate Drive, Suite 400, Burlington, MA 01803, USA.
Willems, P., Vrac, M., 2011. Statistical precipitation downscaling for small-scale hydrological impact investigations of climate change. Journal of Hydrology 402, 193–205.
Zorita, E., von Storch, 1999. The analog method as a simple statistical downscaling technique: comparison with more complicated methods. Journal of Climate 12, 2474–2489.